PENNSTATE

IGNITION AND COMBUSTION CHARACTERISTICS OF METALLIZED PROPELLANTS - PHASE II

Annual Report
(January 1993-December 1993)
NASA Lewis Research Center
Grant No. NAG 3-1044

Prepared by
D. C. Mueller and S. R. Turns

Department of Mechanical Engineering
and
Propulsion Engineering Research Center
The Pennsylvania State University
University Park, PA 16802

January 1994

IGNITION AND COMBUSTION CHARACTERISTICS OF METALLIZED PROPELLANTS - PHASE II

Annual Report
(January 1993-December 1993)

Prepared by
D. C. Mueller and S. R. Turns

Department of Mechanical Engineering
and
Propulsion Engineering Research Center
The Pennsylvania State University
University Park, PA 16802

for

NASA Lewis Research Center

Grant No. NAG 3-1044

Bryan Palaszewski
NASA Technical Officer

January 1994

Summary

Experimental and analytical investigations focusing on aluminum/hydrocarbon gel droplet secondary atomization and its effects on gel-fueled rocket engine performance are being conducted. A single laser sheet sizing/velocimetry diagnostic technique, which should eliminate sizing bias in the data collection process, has been designed and constructed to overcome limitations of the two-color forward-scatter technique used in previous work. Calibration of this system is in progress and the data acquisition/validation code is being written. Narrow-band measurements of radiant emission, discussed in previous reports, will be used to determine if aluminum ignition has occurred in a gel droplet. A one-dimensional model of a gel-fueled rocket combustion chamber, described in earlier reports, has been exercised in conjunction with a two-dimensional, two-phase nozzle code to predict the performance of an aluminum/hydrocarbon fueled engine. Estimated secondary atomization effects on propellant burnout distance, condensed particle radiation losses to the chamber walls, and nozzle two-phase flow losses also investigated. Calculations indicate that only modest secondary atomization is required to significantly reduce propellant burnout distances, aluminum oxide residual size and radiation heat losses. Radiation losses equal to approximately 2-13 % of the energy released during combustion were estimated, depending on secondary atomization intensity. A two-dimensional, two-phase nozzle code was employed to estimate radiation and nozzle two-phase flow effects on overall engine performance. Radiation losses yielded a 1 % decrease in engine I_{sp}. Results also indicate that secondary atomization may have less effect on two-phase losses than it does on propellant burnout distance and no effect if oxide particle coagulation and shear induced droplet breakup govern oxide particle size. Engine I_{sp} was found to decrease from 337.4 to 293.7 seconds as gel aluminum mass loading was varied from 0-70 wt%. Engine I_{sp} efficiencies, accounting for radiation and two-phase flow effects, on the order of 0.946 were calculated for a 60 wt% gel, assuming a fragmentation ratio of 5.

Table of Contents

Program Objectives

The overall objective of our research is to provide an increased understanding of the ignition and combustion characteristics of aluminum gel propellants using a combination of experiment and analysis, and to estimate gel combustion and secondary atomization effects on rocket engine performance through numerical modeling. Specific objectives are as follows:

1. Develop diagnostic techniques to investigate the ignition and secondary atomization of various gels in the droplet size range of practical interest (10-100 μm)

2. Understand the roles of surfactants, gellants, aluminum particle size, and aluminum mass loading on the secondary atomization of aluminum gel droplets

3. Estimate rocket engine performance losses due to gel combustion and determine the effects of secondary atomization on these losses through a one-dimensional model of a gel-fueled rocket combustion chamber and an existing two-dimensional, two-phase flow nozzle code.

4. Perform vehicle mission studies, incorporating the above losses, to estimate the actual performance potential of aluminum/hydrocarbon gel propellants.

Experimental Systems

Limitations of the Two-Color Forward-Scatter Diagnostic Technique

In previous experimental work, a two-color, forward-scatter sizing/velocimetry system was used to determine particle size and velocity in a dilute stream of burning gel droplets.[1-3] He-Ne laser light scattered by a particle is detected by optics oriented at 90° to the laser beam axis and is used to trigger the data acquisition system, ensuring that all measured particles are exposed to the same incident Ar-ion light intensity, thereby permitting a direct correlation of particle diameter with scattered Ar-ion light intensity. Given the Gaussian intensity profile of the He-Ne laser beam, however, a range of trigger voltage levels is expected for a given size particle. Because of inherent electronic noise on the He-Ne trigger channel, a non-zero trigger threshold is required to prevent false acquisition triggering. Given that a small particle scatters less light than a large particle for a given incident light intensity, the effective sampling cross-sectional area in which a small particle can generate a sufficient trigger signal will be less than the sampling area for larger particles. Because the probability of a given particle size being detected is proportional to the sampling cross-sectional area, the small particle population is underrepresented.[1,4] Therefore, the measured particle size distribution is biased towards larger particles and a probability distribution function (PDF) must be applied to the data in order to obtain the true particle size distribution.[1]

By convolving a Gaussian beam profile and a detector slit function profile, Holve[4] derived expressions for both sampling volume and sampling cross-sectional area as functions of system geometry and the light scattering response function, F(d,n), where d is particle diameter and n is the particle complex refractive index. Essentially, F(d,n) is the

ratio of scattered light intensity to incident light intensity. The detector slit function profile was approximated as the exponential expression, $\exp[-2(2x'/W_s)^p]$, where p is determined by the blur spot size of the receiving optics, and coordinate direction x′ is at an angle, θ, to the coordinate x. This arrangement is depicted in Fig. 1.

Based on the above assumption of an exponential slit function profile, the sampling cross-sectional area for a particular particle size, j, can be expressed as follows:

$$S_j = \beta \frac{W_o W_s}{\sin\theta} \left\{ \frac{1}{2} \ln\left[\frac{F(d_j, n)}{F(d_t, n)} \right] \right\}^{\frac{p+2}{2p}} \qquad (1)$$

where β is the system gain, W_0 is the He-Ne beam waist diameter, W_S is the detector slit width, and d_t is the threshold particle diameter that can be detected. This expression can be normalized by dividing by a reference sampling cross-sectional area, S_{ref}, to yield the following:

$$\frac{S_j}{S_{ref}} = \left\{ \frac{\ln\left[F(d_j, n)/F(d_t, n)\right]}{\ln\left[F(d_{ref}, n)/F(d_t, n)\right]} \right\}^{\frac{p+2}{2p}} = \frac{1}{PDF}. \qquad (2)$$

As indicated, Eq. 2 is the inverse of the PDF used to correct for data collection bias.

Although Eq. 2 describes the required PDF, there are still difficulties in determining this expression, the greatest being uncertainty in the particle refractive index, n, and the scattering response function, F(d,n). Light scattering in the 90° direction, unlike near-forward scattering, is highly sensitive to particle refractive index and shape. Since the refractive index of a gel droplet is unknown and changes as the droplet passes through different combustion stages, the scattering response function cannot be accurately determined. In addition, given that the He-Ne beam diameter in the probe volume is 81 μm, the scattering response function cannot be calculated using Mie theory because large droplets are exposed to a non-uniform incident illumination. Holve[4] recommends a beam diameter four times greater than particle diameter for uniform particle illumination, limiting Mie-scattering calculations for the two-color diagnostic system to particles less than 20 μm in diameter.

Single Laser-Sheet Forward-Scatter Sizing/Velocimetry Technique

Based on the above difficulties, a single laser diagnostic technique is being developed, in which all particles pass through a uniform intensity region of a laser sheet, thereby removing any particle size bias in the data collection process. Testing has demonstrated that the gel droplet spray, exiting the burner through a 1.8 mm i.d. tube, maintains an approximately constant diameter of ~2 mm throughout the postflame region. Consequently, the laser sheet must have a uniform intensity region, defined as an intensity variation of less than 2%, large enough to encompass the entire gel particle spray. Calculations indicate that a $1/e^2$ sheet width of ~36 mm provides a 4 mm diameter uniform

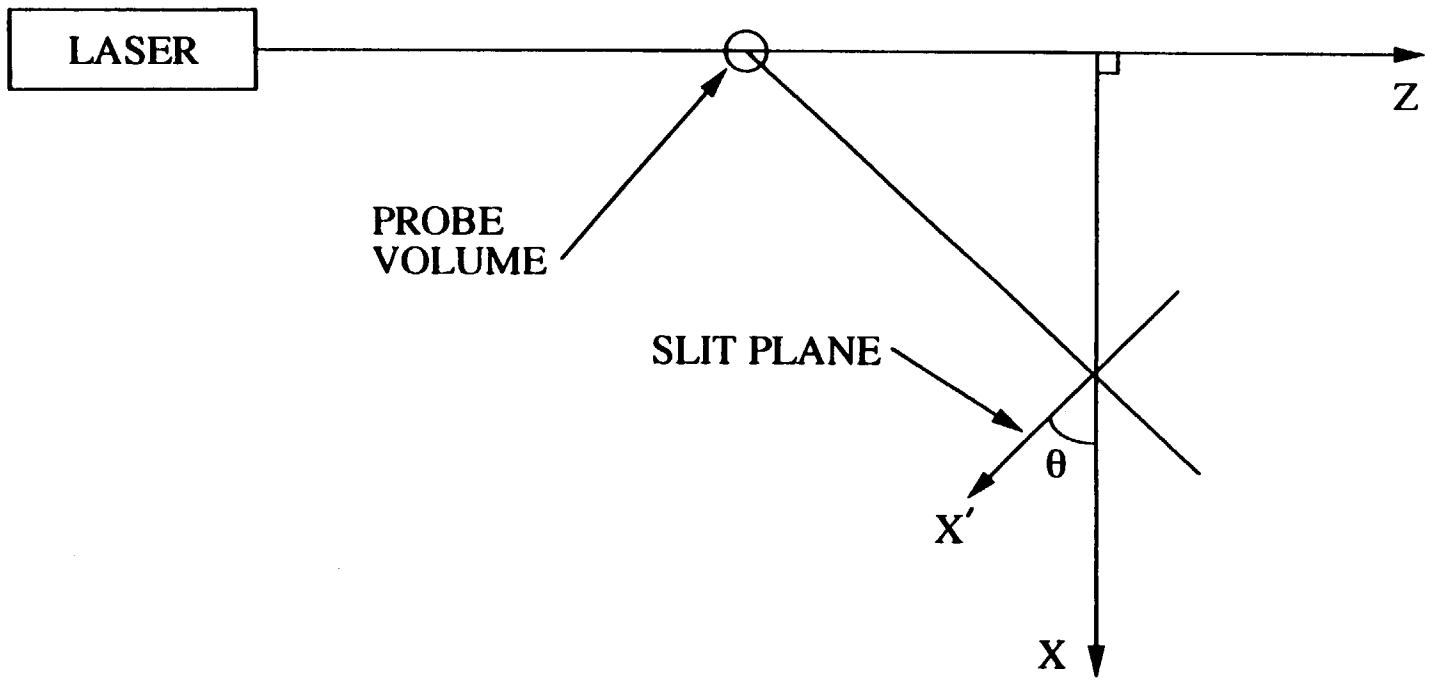

Figure 1. Schematic of coordinates used in Holve's calculation of sample volume cross-sectional area.

intensity region, which should encompass the 2 mm diameter droplet spray mentioned above, including particles ejected by secondary atomization.

A schematic of the single laser sheet system and resulting laser sheet are presented in Figs. 2 and 3, respectively. In brief, a 1.1 mm beam of a He-Ne laser (Spectra-Physics 124B) is passed through a 750 mm focal length plano-convex spherical lens (L1, Oriel 40815) and a 19 mm focal length plano-convex cylindrical lens (L2, Newport CKX019), producing a horizontal laser sheet over the burner. This sheet has a calculated $1/e^2$ thickness of 550 μm and a sheet width of 36 mm at the focal point of the 750 mm lens. These dimensions are depicted in Fig. 3. Gel particles passing through this sheet scatter light, which is collected in the near-forward direction and collimated by a 350 mm plano-convex spherical lens (L3, Oriel 40800) with a strip of flocking material across its center to block the direct laser light. This collimated light is then focused on a 200 μm horizontal slit (S1) by a second 350 mm lens (L4, Oriel 40800). Light passing through this slit is then separated into two components by a beam splitter cube (BS1, Melles-Griot 03-BSC-009). The first component, used for particle sizing, passes through a 632.8 nm line filter (F1, Oriel 52720) and enters a PMT (Hamamatsu R928) where the particle sizing signal is generated. The second component, used to detect aluminum combustion, passes through a 400 nm narrow bandpass filter (F2, Oriel 53800) and enters a second PMT (Hamamatsu R928) to produce the aluminum combustion signal. A two-channel 20 MHz A/D acquisition board (Rapid Systems 2040) will be used to sample the above signals and a 486 33 MHz personal computer will be employed for signal validation and data analysis computations.

Maximum Sample Number Density: Using the above diagnostic system, only data obtained from single particle light scattering provides a correct measure of particle size and velocity. If two or more particles are simultaneously present in the sample volume, the data is invalid and must be rejected. Because high rejection rates slow the acquisition process, a probability analysis must be performed to evaluate likely data rejection rates given particle number density in the flow and the sample volume size.

Since the probability of a particle being in the sample volume at a given time is statistically independent of other particles being present, the probability, P(n,x), of n additional particles being simultaneously present when a given particle is in the probe volume is given by the Poisson distribution[5]

$$P(n,x) = \frac{x^n \exp(-x)}{n!} \tag{3}$$

where

$$x \equiv \sum_{i=1}^{m} C_i \tau \tag{4}$$

In the above summation, τ represents particle residence time in the control volume, m is the number of droplet size classes and C_i is the count rate for the i^{th} size class. Given that data are only valid if no additional particles are present (i.e., n=0), and that the sum of all

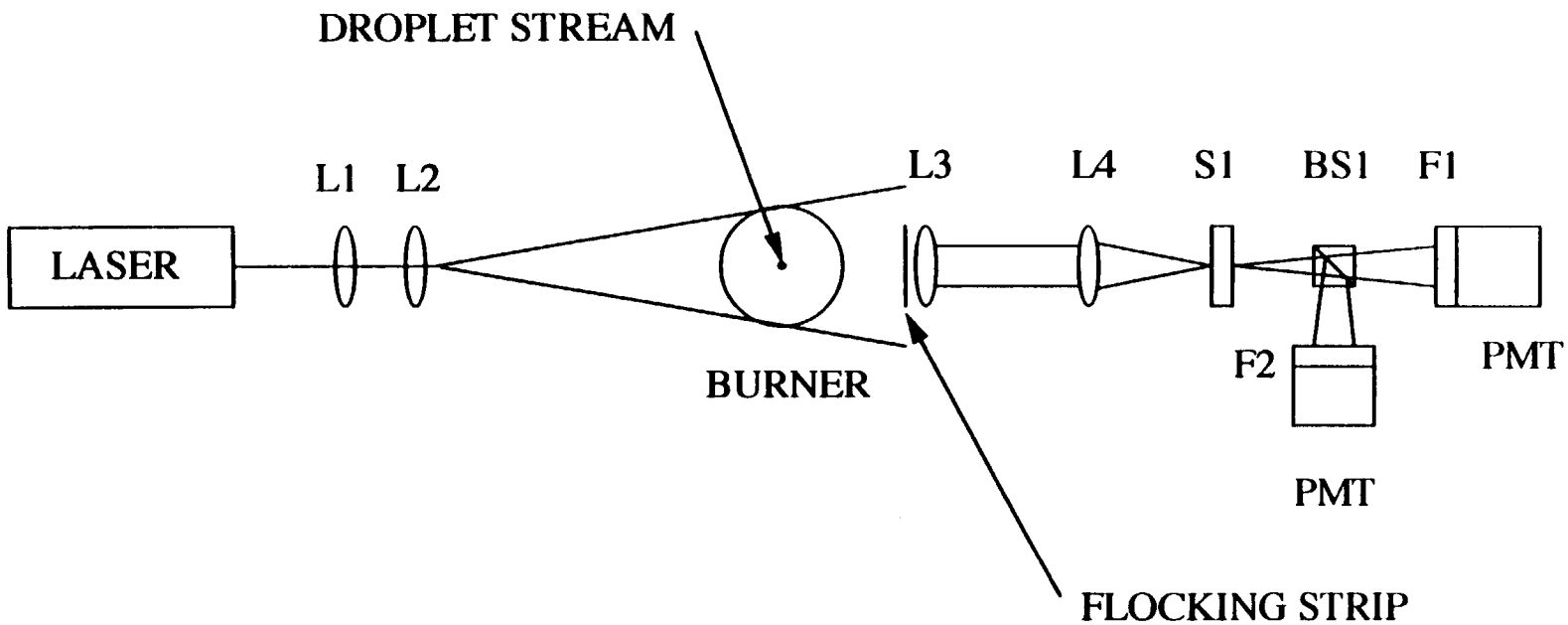

Figure 2. Schematic of the laser sheet forward-scatter diagnostic technique for droplet size and velocity measurements and aluminum combustion detection.

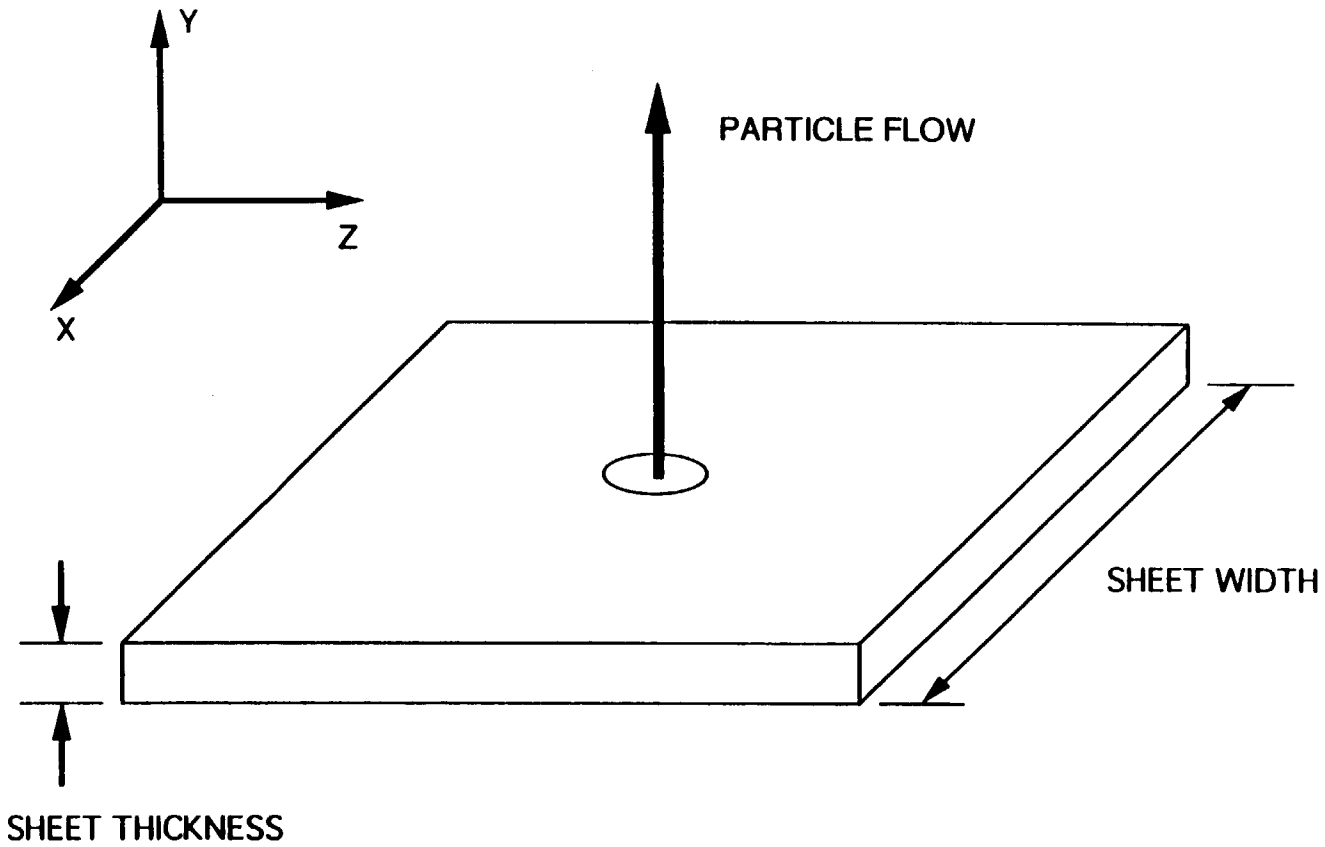

Figure 3. Schematic of the laser sheet in the diagnostic sample volume region.

probabilities must equal unity, the probability of more than one particle being simultaneously present in the sample volume can be expressed as[5]

$$P_{sum} = 1 - \exp\left(-\sum_{i=1}^{m} C_i \tau \right) \tag{5}$$

The particle count rate, C_i, can be related to the particle number density through the relation, $C_i = U \cdot S_i \cdot N_i$, where U is particle velocity, S_i is the probe cross-sectional area for particle size i, and N_i is the i^{th} size class number density. Since our diagnostic technique employs a sample volume of uniform light intensity, S_i is the same for all particle sizes. Substituting the above relation for C_i, and assuming that probe volume residence time is independent of particle size, Eq. 5 becomes

$$P_{sum} = 1 - \exp\left(-U\tau S \sum_{i=1}^{m} N_i \right) \tag{6}$$

Furthermore, the probe volume residence time, τ, represents the time a particle takes to cross the laser sheet, t/U, where t is the sheet thickness. Using this relation and realizing that the probe sample volume $V_p = t \cdot S$, Eq. 6 can be rewritten as

$$P_{sum} = 1 - \exp\left(-V_p N_T \right) \tag{7}$$

where N_T is the total particle number density. Figure 4 illustrates the effect of particle number density on the probability of n additional particles being in the sample volume. For n=0, no interfering particles are present in the sample volume. Therefore, the probability of n=0 represents the probability of obtaining a valid data point. Based on experience with the two-color forward scatter system,[2,3] data rejection rates should be acceptable for particle number densities of up to 1000 particles/cc.[1] Although this number density should prove adequate for our needs, experimental testing will be needed to provide verification.

Theoretical Engine Performance Analysis

One-Dimensional Combustor Model Description

As developed in previous reports, a one-dimensional model of a JP-10/Al/O_2(gaseous) fueled rocket combustor has been developed to evaluate secondary atomization effects on propellant combustion.[6,7] In brief, a radially uniform spray, consisting of four droplet size classes, enters the combustion chamber and burns in a process incorporating liquid carrier burnout, droplet secondary atomization, aluminum agglomerate heat up and combustion, two-phase particle flow, and radiation from solid combustion products to the chamber walls. A schematic of the gel combustion process for a single droplet, with and without secondary atomization, is presented in Fig. 5. Because the post-secondary atomization droplet size distributions are currently unknown, droplets are assumed to fragment into a

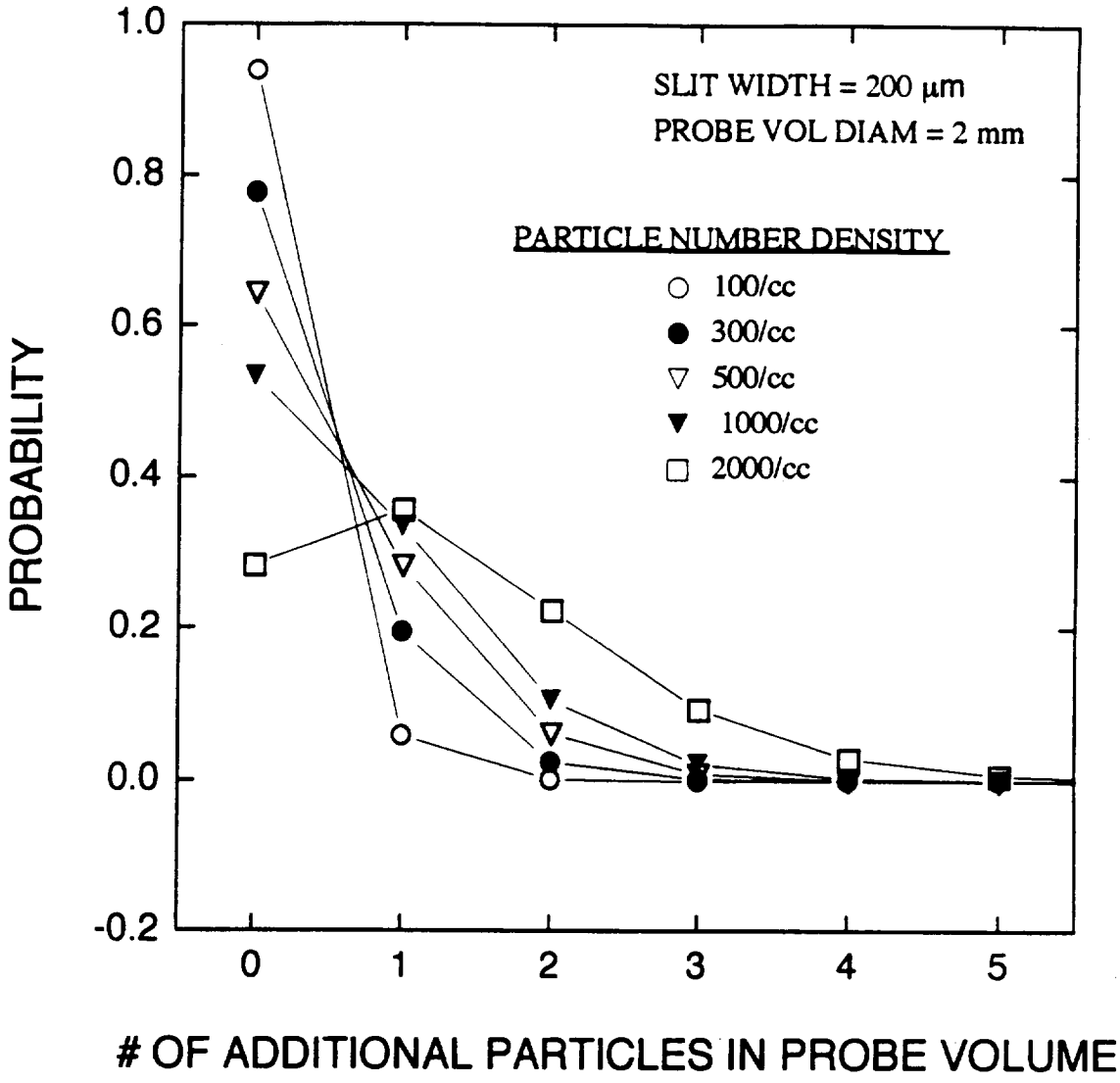

Figure 4. Effect of particle number density on the probability of having n additional particles in the probe sample volume. Results assume a 2 mm diameter droplet stream.

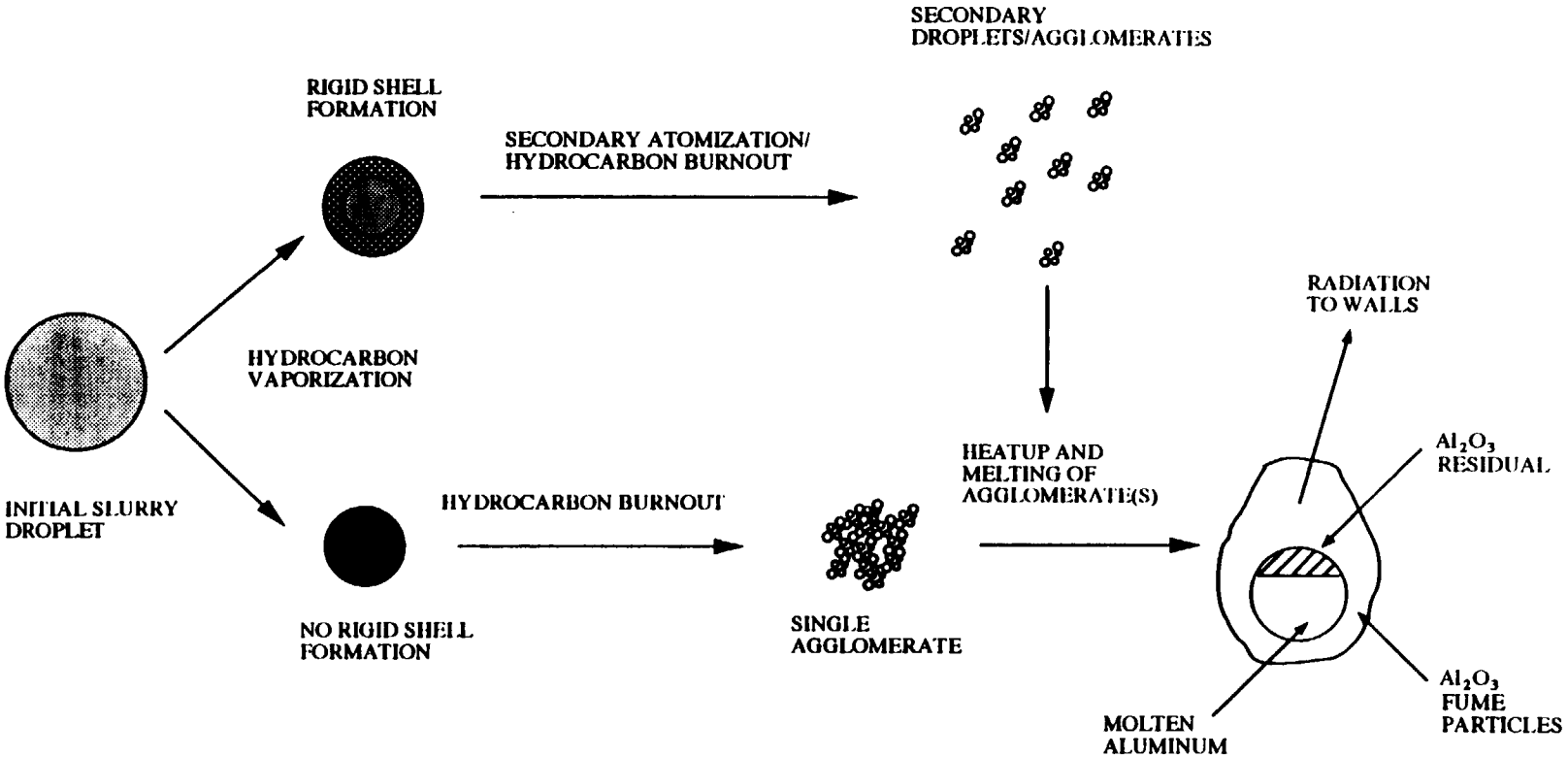

Figure 5. Schematic of the gel droplet combustion process in a combustion chamber, with and without droplet secondary atomization.

given number of equal-sized droplets where the number of secondary droplets produced per initial droplet is defined as the fragmentation ratio, β, which is treated as a model parameter.

Radiation Modeling: A detailed development of the condensed product radiation model used in the combustor code is presented in prior reports,[6,7] but further clarification of this radiation model is required. In our earlier report,[7] the final equation representing radiation heat flux from the condensed products to the chamber walls was expressed as

$$q^r(R) = \sum_{n=1}^{L} \frac{4I_1(R/\xi_n)}{3\xi_n I_o(R/\xi_n) + 2I_1(R/\xi_n)} \cdot \left\{ F_n(T_g)\sigma T_g^4 - F_n(T_w)T_w^4 \right\}, \qquad (8)$$

where n represents a wavelength interval; I_o and I_1, Modified Bessel functions; ξ, a function of particle optical properties; T_g, the gas temperature; T_w, the chamber wall temperature; and $F_n(T)$, the fraction of total radiation emitted by a blackbody at temperature T in the wavelength interval between λ_n and λ_{n+1}. The variable R was defined as the chamber radius. It should be clarified that R is actually the chamber radius in terms of flow optical thickness and should be defined as $R = (a + \sigma_s)\mathbf{R}$, where $\boldsymbol{R}$ is the physical chamber radius and the variables, a and σ_s, are the absorption and scattering coefficients of the flow.

One-Dimensional Combustor Model Results

The one-dimensional combustor code was exercised using the conditions presented in Table 1. These values were chosen to simulate an upper-stage booster and represent the maximum I_{sp} operating point for a 60 wt% aluminum gel. Because propellant mass flow rate is governed in part by nozzle geometry, the Solid Propellant Performance Prediction Code (SPP)[8] was used to determine the propellant mass flow rates. Since an appropriate spray distribution remains to be determined from gel atomization research, the arbitrary normalized droplet size distribution presented in Fig. 6 was used.

Table 1: Model Operating Conditions	
Chamber Diameter	0.19 m
Chamber Pressure	38 atm
Liquid Carrier	JP-10
Gel Aluminum Mass Loading	60%
Gel Flow Rate	10.78 kg/s
Oxidizer Flow Rate	11.75 kg/s
Chamber Wall Temperature	1000 K

Gas temperature and composition, assuming a fragmentation ratio, β, of 5 are presented in Fig. 7. The jagged shape of both the temperature and composition profiles arise from using only four droplet size classes instead of a continuous droplet size distribution. The slow rate of temperature increase in the region between 0.1 and 0.25 m is caused by the large enthalpy transfer from the gas flow to heat the aluminum after hydrocarbon burnout.

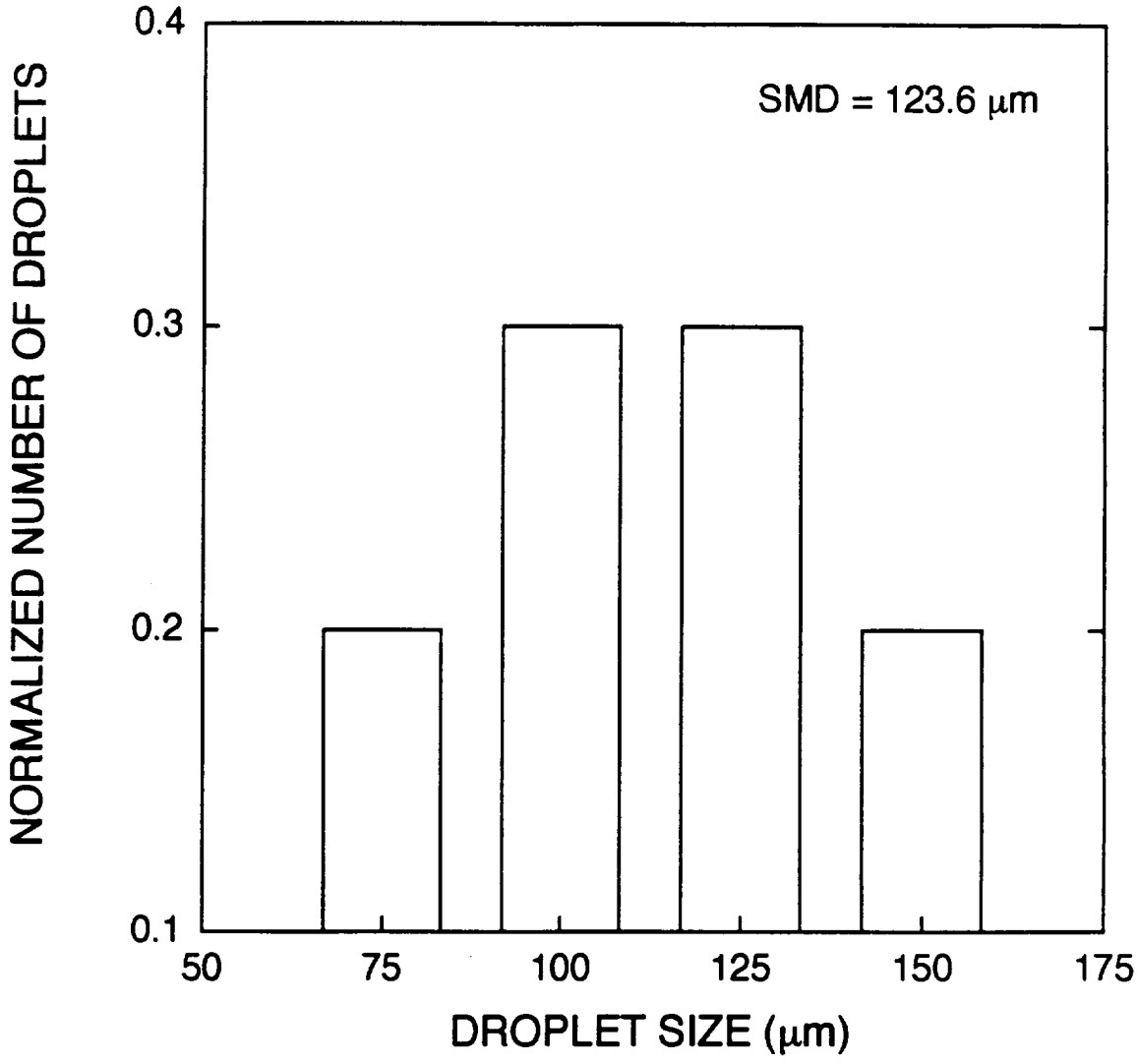

Figure 6. Normalized droplet size distribution used in the combustor code.

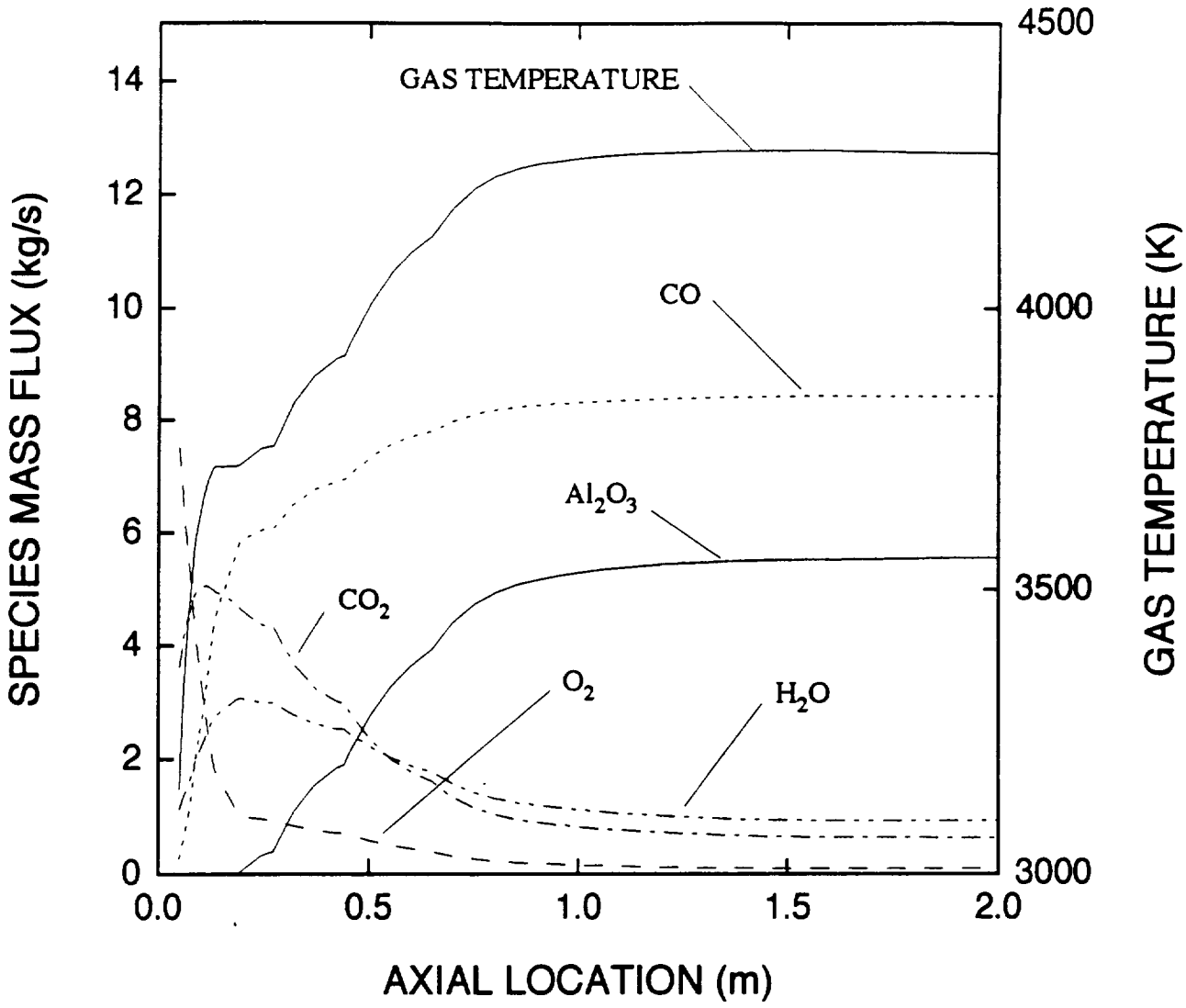

Figure 7. Gas temperature and major species mass fluxes versus axial location. Data are for a 60 wt% aluminum gel assuming a fragmentation ratio of 5.

In Fig. 8, propellant burnout distance is plotted versus fragmentation ratio, β, to illustrate the potential benefits of secondary atomization in reducing required engine residence times. It is readily apparent that only modest secondary atomization is required to significantly reduce propellant burnout distance, and that higher secondary atomization intensities, represented by larger fragmentation ratios, have a marginal effect.

Final oxide residual diameter as a function of fragmentation ratio is shown in Fig. 9. Similar to the trend seen in propellant burnout distance, moderate secondary atomization intensities significantly reduce final Al_2O_3 residual diameter, with greater secondary atomization intensities providing decreasing marginal reductions in residual diameter. The final Al_2O_3 weight distribution as a function of particle size is plotted in Fig. 10. The bi-modal size distribution associated with aluminum combustion[9,10] is readily apparent as well as the decrease in residual particle size caused by secondary atomization. It should be noted that secondary atomization has no effect on the size of the sub-micron fume particles produced through vapor-phase oxidation of the aluminum.

Radiation losses from condensed combustion products to the chamber walls as functions of fragmentation ratio and aluminum mass loading are shown in Fig. 11. Chamber operating conditions are those that produce maximum I_{sp} for each aluminum mass loading. Radiation losses were found to be strongly influenced by the fragmentation ratio, primarily due to changes in propellant burnout distance. Increasing the gel aluminum mass loading for a given fragmentation ratio was also found to increase radiation losses because of increased chamber temperature and slight increases in propellant burnout distance with increasing aluminum mass loading. Radiation losses were approximately equal to 2-13 % of the energy released during combustion, depending on the aluminum mass loading and the fragmentation ratio.

It should be cautioned that the above radiation heat transfer calculations are only approximate. Axial radiation heat transfer, which has been neglected, may alter the droplet combustion process and/or the actual radiation losses. In addition, research[11] has indicated that the optical properties of the condensed combustion products can vary considerable depending on propellant composition and oxidizer/fuel mixture ratio.

SPP Modeling of Nozzle Two-Phase Flow and Engine Performance

Two-phase flow effects in the engine nozzle were estimated using the SPP nozzle code,[8] which contains two solution modules for determining nozzle performance. The first module provides a transonic analysis of the converging and throat region of the nozzle, and the second module provides a Method of Characteristics (MOC) solution of the supersonic portion of the nozzle. This MOC module incorporates the following assumptions:

- Gas and particle properties are variable
- Energy transfer between the gas and particles is only through convection
- Oxide particles are spherical
- Particles do not interact
- Mass is not transferred between the particles and the gas
- Condensed phase occupies negligible volume in the flow

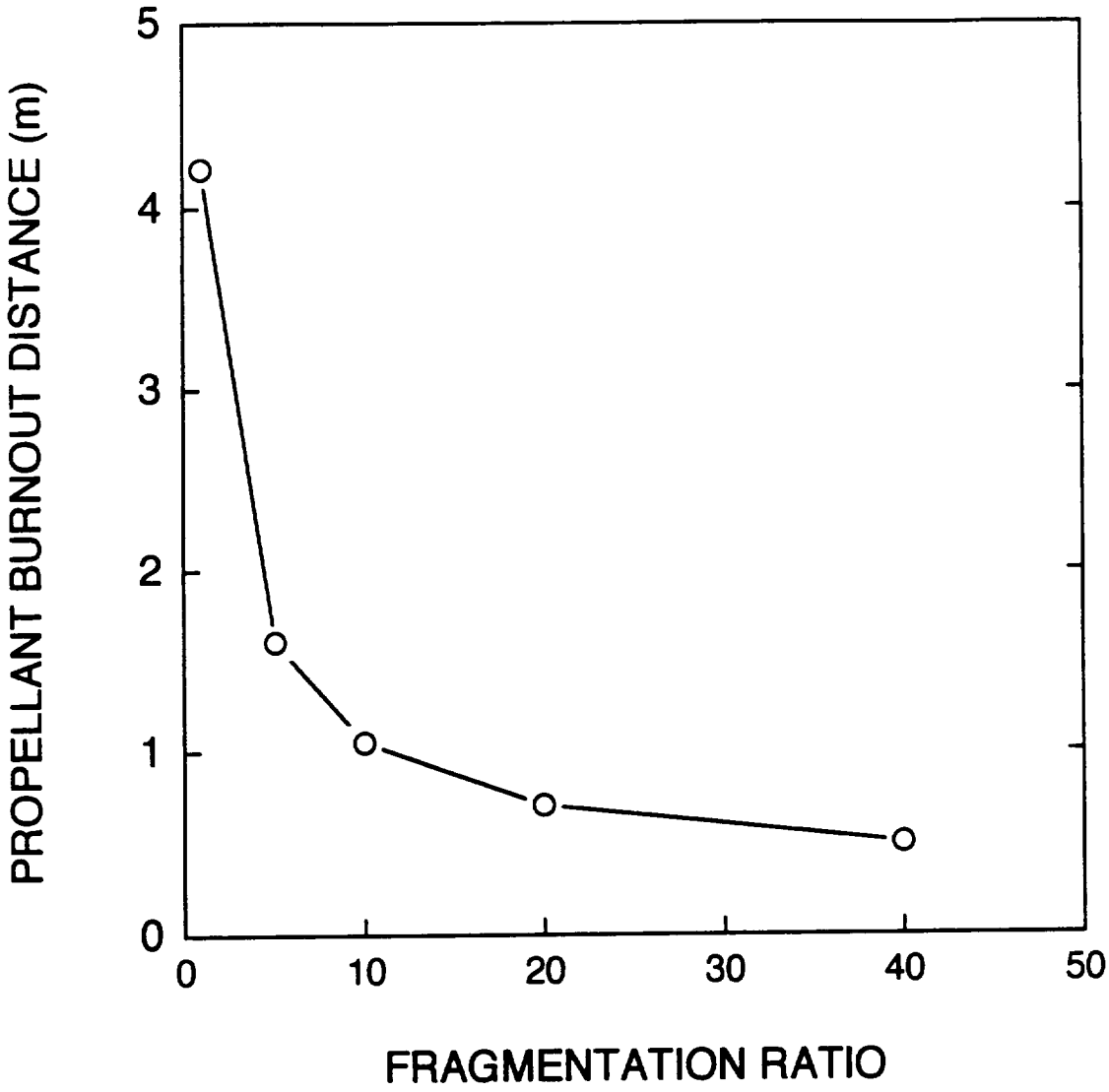

Figure 8. Propellant burnout distance as a function of secondary atomization fragmentation ratio for a 60 wt% aluminum gel.

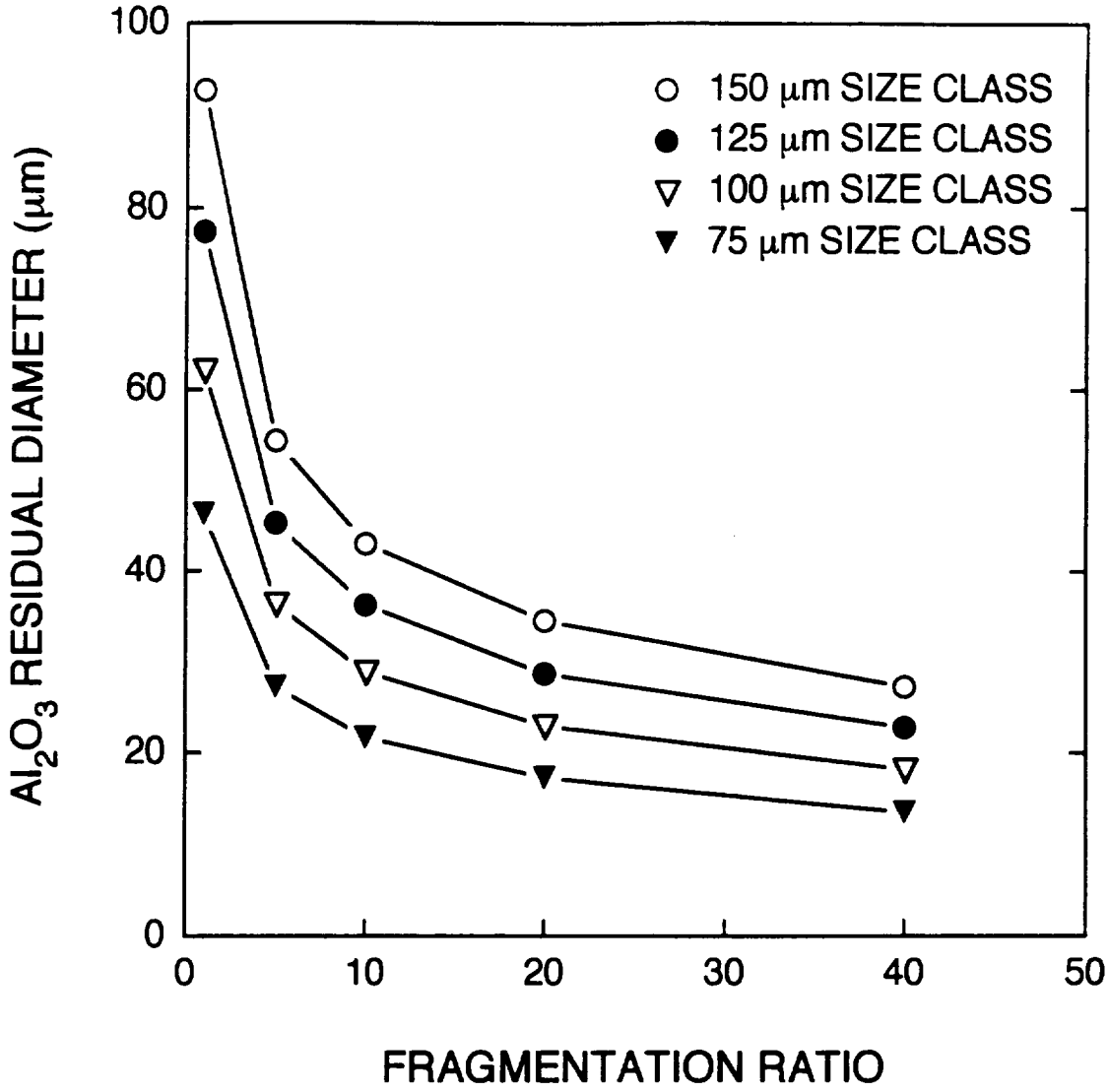

Figure 9. Final oxide residual diameter as a function of secondary atomization ratio for a 60 wt% aluminum gel.

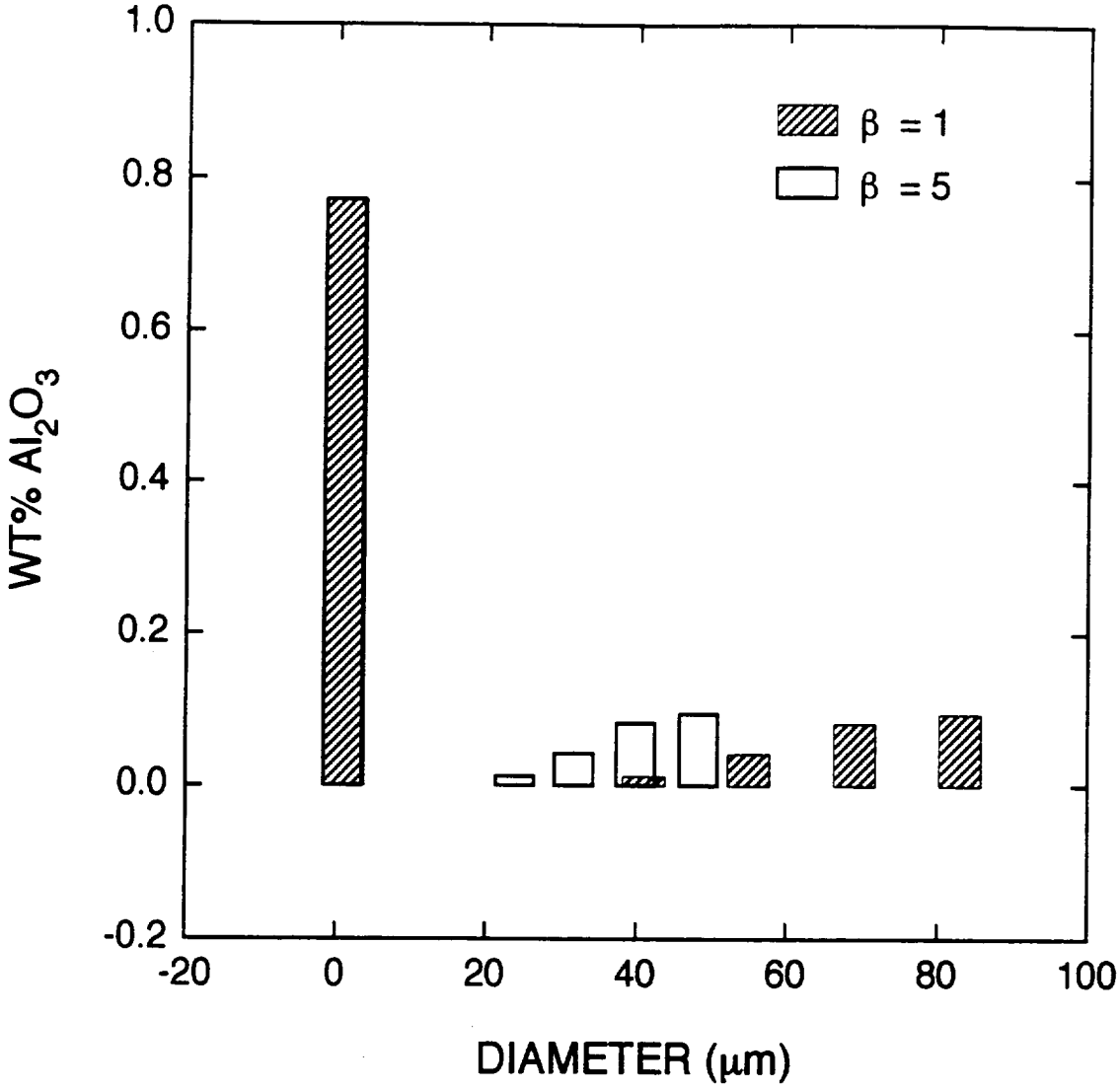

Figure 10. Aluminum oxide weight fraction versus particle diameter for a 60 wt% aluminum gel.

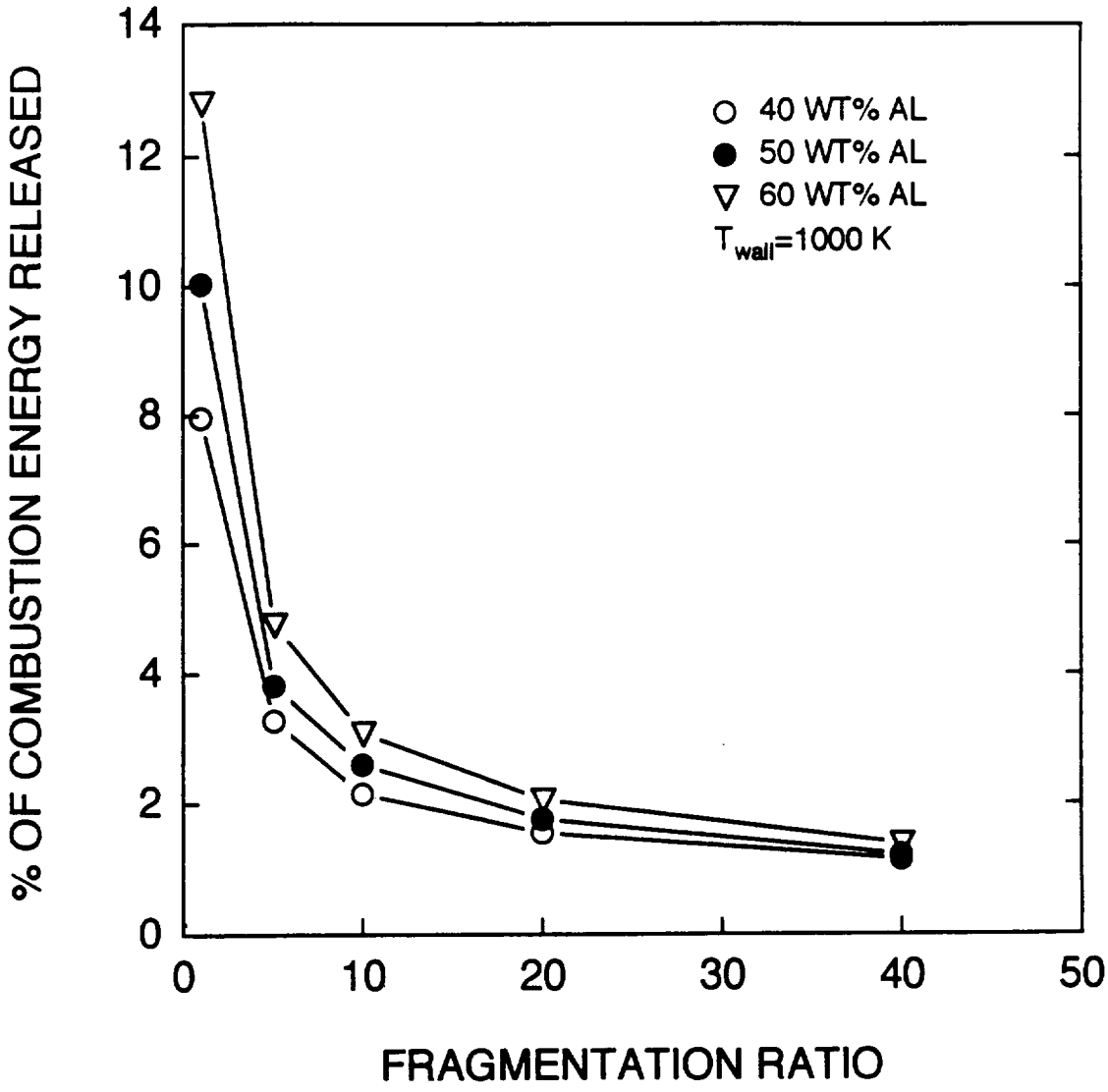

Figure 11. Radiation heat loss as a percentage of combustion energy released as a function of fragmentation ratio and gel aluminum mass loading.

It should be noted, however, that because particle interaction and mass transfer between the particles and gas are neglected in the SPP code, the Al_2O_3 residual size distribution predicted by the combustor code may not be correct for nozzle performance calculations. Since the Al_2O_3 particles are molten throughout most of the nozzle, and because small particles accelerate more quickly than large particles, particle size may increase through coagulation.[12] Similarly, additional Al_2O_3 may be produced through the recombination of gas-phase radicals as the exhaust gases cool during expansion, resulting in the nucleation of additional particles and/or growth of previously formed particles.[13] Particle size may also decrease due to shear breakup of droplets, particularly in the throat region of the nozzle.[14]

Because of these uncertainties in Al_2O_3 particle size, two methods of estimating particle size, which should bound the true particle size, are used in the evaluation of nozzle performance. In the first method, we use an Al_2O_3 particle size distribution that is determined by the one-dimensional combustor code, making secondary atomization the primary mechanism governing particle size. In the second method, secondary atomization is assumed to have no effect on mean particle size; rather, coagulation, particle surface growth, and shear induced droplet breakup are assumed to be the dominate mechanisms affecting particle size. Assuming that these coagulation and breakup mechanisms are comparable to those in solid nozzles, the following solid motor correlation of mass median Al_2O_3 particle diameter, $\overline{D}_{43}$, as a function of nozzle diameter, D_t, was employed:[8]

$$\overline{D}_{43} = 3.63 D_t^{.2932} \tag{9}$$

resulting in a particle mass median diameter of 5.6 μm.

Engine Performance Results

A comparison of two-phase flow effects on I_{sp} for the above methods of determining Al_2O_3 particle size are presented in Fig. 12 for a 60 wt% aluminum gel. As seen here, secondary atomization may reduce two-phase flow losses but not as significantly as propellant burnout distance (4% versus 62%, cf. Fig. 3). To illustrate the separate contributions of radiation and two-phase losses, radiation losses were incorporated in the case represented by the dashed line. Given a fragmentation ratio of 5, radiation losses yield a decrease in I_{sp} of approximately 1% compared to the 4% resulting from two-phase losses.

Using the solid motor correlation for particle size, I_{sp} was calculated for a range of aluminum mass loadings and propellant mixture ratios and compared with I_{sp} calculations for a JP-10/O_2 bi-propellant. Figure 13 shows that I_{sp} decreases with increasing aluminum mass loading and that the maximum I_{sp} mixture ratio becomes richer, as has been predicted by other studies,[15,16] although the I_{sp} decrease is significantly greater with the incorporation of radiation and two-phase flow losses.

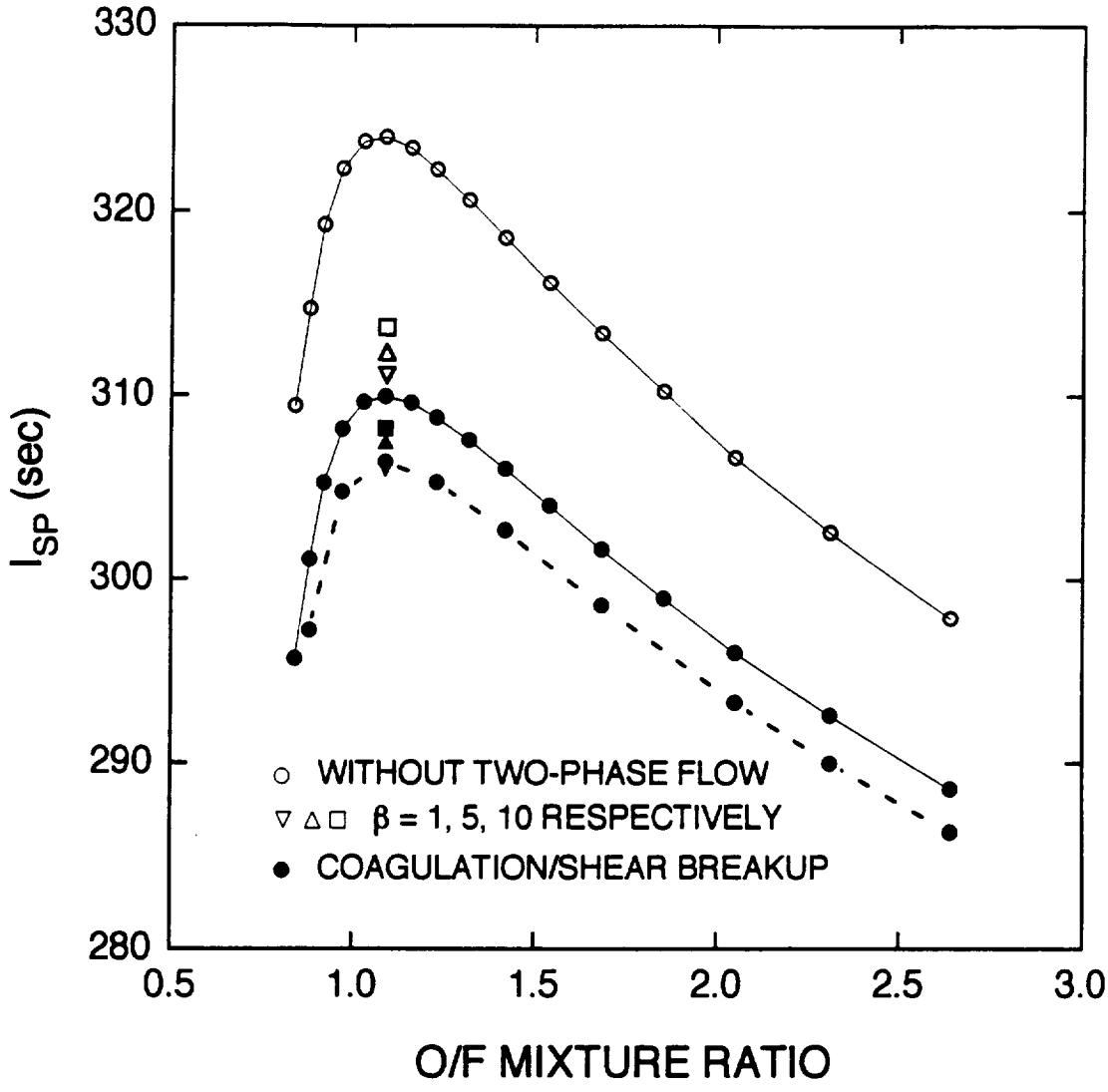

Figure 12. Engine I_{sp} as a function of oxide particle size model and O/F mixture ratio for a 60 wt% aluminum gel. Dashed line indicates inclusion of radiation losses. Model assumes an Extended Delta nozzle profile.

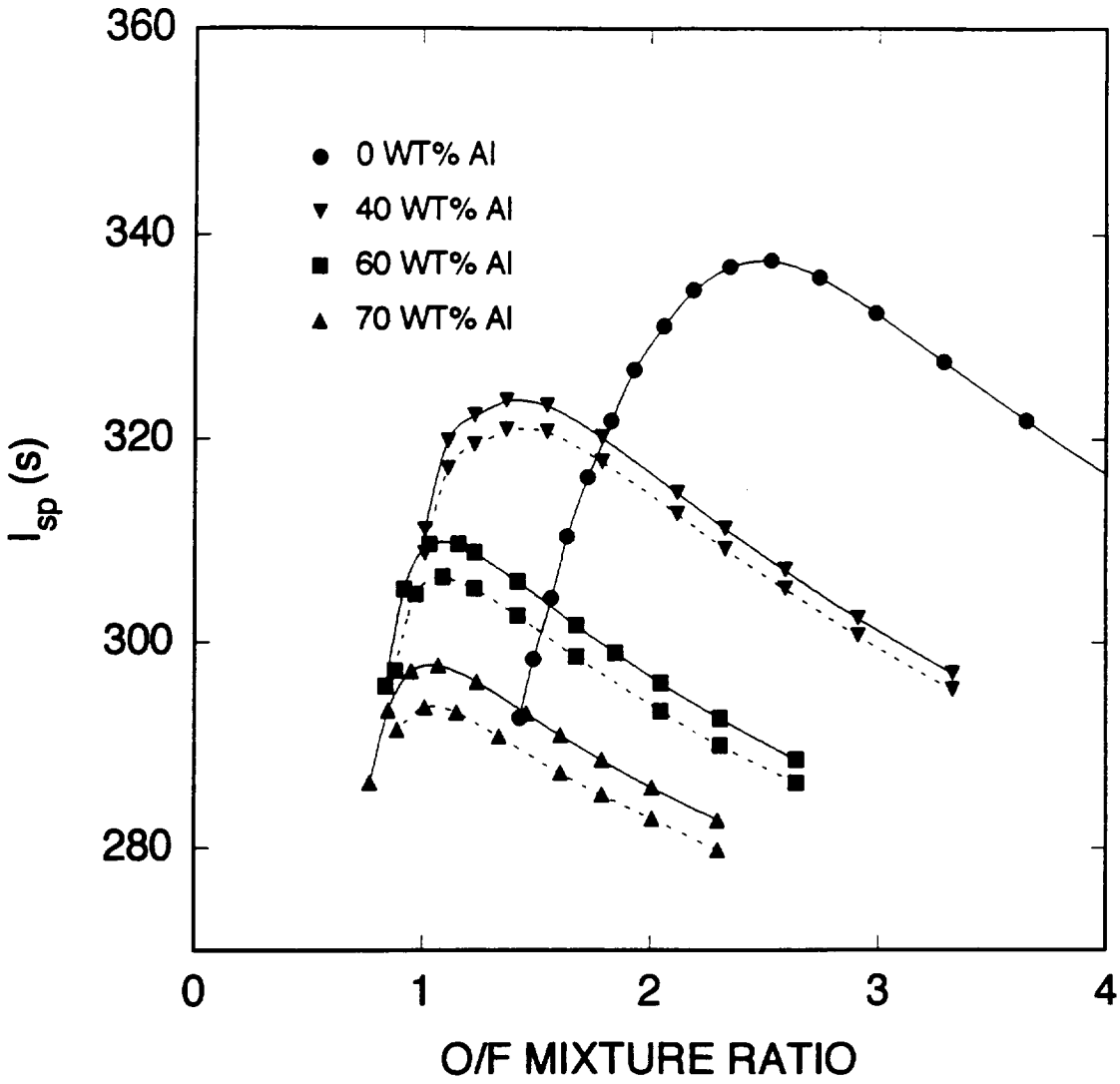

Figure 13. Engine I_{sp} as a function of O/F mixture ratio and gel aluminum mass loading. Dashed lines represent inclusion of radiation losses.

Conclusions

Based on the above experimental and theoretical work, the following results were obtained:

1. A single laser-sheet sizing/velocimetry technique has been developed to overcome limitations in the two-color, forward-scatter diagnostic technique used in previous work. This system has been constructed and is now being calibrated. Data acquisition/validation software is currently being written to operate this system.

2. Exercise of the one-dimensional combustor model predicts that only moderate secondary atomization (β=5) is required to reduce overall propellant burnout distance by 62% and final Al_2O_3 residual diameter by 41%.

3. Radiation losses for a 60 wt% gel, assuming β=5, are estimated to be approximately 5 % of the energy released during combustion, resulting in a 1% decrease in engine I_{sp}. Secondary atomization may reduce radiation heat transfer losses, primarily due to decreases in the propellant burnout distance. For example, a fragmentation ratio of five results in a 61 % decrease in radiation losses. Radiation losses were also found to be a function of gel composition and engine operating conditions, as a result of changes in chamber temperature.

4. Two-dimensional, two-phase nozzle code results indicate that secondary atomization may have little effect on nozzle two-phase flow losses. Specifically, a fragmentation ratio of 5 decreases two-phase flow losses by only 4 % compared to the above 62% reduction in propellant burnout distance. Furthermore, secondary atomization may have no effect on two-phase flow losses if particle coagulation, surface growth, and shear induced breakup are the dominant mechanisms controlling oxide particle size.

Future Work

1. Calibrate single-laser diagnostic apparatus and complete the data acquisition code.

2. Perform a parametric study of aluminum mass loading and surfactant concentration effects on limiting droplet size for secondary atomization and post-secondary atomization particle size distributions.

3. Numerically model the burning droplet spray used in the above experiments using a modified version of the one-dimensional combustor code to aid in differentiating between normal droplet combustion and secondary atomization.

4. Using data collected in the above work, incorporate a realistic post-secondary atomization model in the one-dimensional combustor code and using the combustor code and SPP, evaluate the potential of gel-fueled engine performance and secondary atomization effects on this performance.

5. Develop a realistic Earth-to-LEO mission analysis to estimate the performance potential of hydrocarbon gel fueled vehicles.

References

1. Wang, J. C., and Hencken, K. R., "In Situ Particle Size Measurements Using a Two-Color Laser Scattering Technique," *Applied Optics*, Vol. 25, March 1986, pp. 653-657.

2. Turns S. R., Mueller, D. C., and Scott, M. J., "Ignition and Combustion Characteristics of Metallized Propellants: Semi-Annual Report," to NASA Lewis Research Center, Grant No. 3-1044, January 1990.

3. Mueller, D. C. and Turns, S. R., "Ignition and Combustion Characteristics of Metallized Propellants: Semi-Annual Report," to NASA-Lewis Research Center, Grant No. 3-1044, September 1991.

4. Holve, D. J., Tichenor, D., Wang, J. C., and Hardesty, D. R., "Design Criteria and Recent Developments of Optical Single Particle Counters for Fossil Fuel Systems," *Optical Engineering*, Vol. 20, Jul/Aug 1981, pp. 529-539.

5. Holve, D. J., and Self, S. A., "Optical Particle Sizing for In Situ Measurements- Part 1", *Applied Optics*, Vol. 18, May 1979, pp. 1632-1645.

6. Mueller, D. C., and Turns, S. R., "Ignition and Combustion Characteristics of Metallized Propellants: Annual Report," to NASA-Lewis Research Center, July 1992.

7. Turns, S. R., and Mueller, D. C., "Ignition and Combustion Characteristics of Metallized Propellants: Final Report - Phase I," to NASA-Lewis Research Center, Grant No. 3-1044, January 1993.

8. Nickerson, G.R., et. al., "The Solid Propellant Rocket Motor Performance Prediction Computer Program (SPP), Version 6.0," AFAL/TSTR, Edwards AFB, CA, Dec 1987.

9. Kraeutle, K.J., "Particle Size Analysis in Solid Propellant Combustion Research," *Progress in Astronautics and Aeronautics*, Vol. 53, 1977, pp. 449-463.

10. Salita, M., "Quench Bomb Investigation of Al_2O_3 Formation From Solid Rocket Propellants (Part II): Analysis of Data," *25th JANNAF Combustion Meeting*, Oct. 1988, pp. 185-197.

11. Konopka, W. L., Reed, R. A., and Calia, V. S., "Measurements of Infrared Optical Properties of Al_2O_3 Rocket Particles," *Progress in Astronautics and Aeronautics*, Vol. 91, AIAA, New York, 1984, pp. 180-196.

12. Crowe, C. T., and Willoughby, P. G., "A Study of Particle Growth in a Rocket Nozzle," *AIAA Journal*, Vol. 5, July 1967, pp. 1300-1304.

13. Courtney, W. B., "Condensation in Nozzles," Ninth Symposium (International) on Combustion, The Combustion Institute, Pittsburgh, 1963, pp. 799-810.

14. Bartlett, R. W., and Delaney, L. J., "Effect of Liquid Surface Tension on Maximum Particle Size in Two-Phase Nozzle Flow," *Pyrodynamics*, Vol. 4, 1964, pp. 337-341.

15. Yatsuyanagi, N., Sakamoto, H., Sato, K., Ono, F., Tamura, H., and Moro, A., "Combustion Characteristics of Metallized Hydrocarbon Fuels," 17th International Symposium on Space Technology and Science, Tokyo, Japan, May 1990.

16. Zurawski, R. L., and Green, J. M., "An Evaluation of Metallized Propellants Based on Vehicle Performance," AIAA Paper 87-1773, June-July 1987.